*Korean J. Chem. Eng.*, 38(10), 2150-2156 (2021)
DOI: 10.1007/s11814-021-0839-8

pISSN: 0256-1115
eISSN: 1975-7220

# Preparation of heteroatom isomorphously substituted MEL zeolite membranes for pervaporation separation of dimethylformamide/water mixtures

**Qigang Wu*, Rong Xu**, Hui Shao**, Jing Zhong**,†, Xiuxiu Ren**, and Zhengzhong Zhou***

*National & Local Joint Engineering Research Center of Biomass Refining and High-Quality Utilization, Institute of Urban & Rural Mining, Changzhou University, Changzhou 213164, China
**Jiangsu Key Laboratory of Advanced Catalytic Materials and Technology, School of Petrochemical Engineering, Changzhou University, Changzhou 213164, China
(*Received 30 January 2021 • Revised 26 April 2021 • Accepted 10 May 2021*)

**Abstract**−The recovery of dimethylformamide (DMF) by pervaporation is less energy intensive and more economical than the traditional distillation method. High/pure silica zeolite is a typical organics perm-selective material for pervaporation membrane due to its hydrophobic nature, demonstrating great potential for recovering organic components from aqueous solutions. In this study, as an attempt to further enhance the membrane hydrophobicity, titanium and zirconium-substituted MEL type zeolite membranes (Ti-silicalite-2 and Zr-silicalite-2) were synthesized on the $\alpha$-$Al_2O_3$ discs by a secondary growth method. X-ray diffraction (XRD) and Fourier transform infrared spectroscopy (FTIR) results confirmed the isomorphous substitution of the MEL framework by Ti and Zr atoms. The effects of isomorphous substitution, feed temperature and concentration on the DMF recovery performance were investigated via systematically designed pervaporation experiments. The fluxes and separation factors both increased with the isomorphous substitution of heteroatom, as well as increasing feed temperature and decreasing feed concentration. The Ti-silicalite-2 membrane exhibited a high separation factor of 6.4 with a total flux of 0.98 $kg \cdot m^{-2} \cdot h^{-1}$ for a 5 wt% DMF/water feed at 343 K.

Keywords: MEL Zeolite Membrane, Pervaporation, Hydrophobic, Isomorphous Substitution, Dimethylformamide/Water Mixtures

## INTRODUCTION

Dimethylformamide (DMF) is an important industrial chemical that is widely used in the production of synthetic leather and polyurethane products [1]. Because DMF is highly soluble in water, it is easily released into air and water. Considering the high carcinogenicity of DMF to human beings, the recovery of DMF from aqueous solution is essential. The traditional distillation method to recover DMF has the disadvantage of high energy consumption and cost. Pervaporation as a fast-growing separation technology attracts much attention due to its high separation efficiency, less environmental pollution, low energy consumption, and cost saving [2,3]. So far, different types of membranes have been prepared to separate organic/water binary mixture by pervaporation [4-7]. Some of these membranes show excellent pervaporation dehydration performance, such as NaA zeolite membrane and CHA zeolite membrane [8,9]. However, organic perm-selectivity membranes still need to increase separation performance for further industrial application.

Zeolite membrane has great potential in pervaporation due to its unique characteristics such as specific pore structure, good adsorption properties as well as superior mechanical, chemical and biological stability [2,10]. Up to now, many different types of zeolite membranes have been prepared to separate liquid mixtures by pervaporation, such as BEA [11], LTA [12], FAU [13], MOR [14] and MFI [15] membranes. The isomorphous substitution of heteroatom into zeolite membrane is considered to be an effective method to improve its hydrophobicity due to changes in the T-O length and T-O-T angles (T=Si or heteroatom) [16-20]. In the past few years, some researchers have devoted themselves to the synthesis of heteroatom isomorphously substituted zeolite membrane. In particular, MFI zeolite membrane is one of the most studied membranes because of its special framework structures and tunable Si/Al ratio, which determines the hydrophobicity. Bowen et al. [16] incorporated boron into MFI zeolite framework by isomorphous substitution and the results demonstrated that the separation factor of B-ZSM-5 membrane deposited on $Al_2O_3$-coated SiC multi-channel monolith reached 75 with the fluxes of 0.071 $kg \cdot m^{-2} \cdot h^{-1}$ for 1-propanol aqueous solutions at 333 K. Sun et al. [18] prepared stannum isomorphously substituted MFI zeolite membranes deposited on the porous $\alpha$-$Al_2O_3$ tube. The Sn-ZSM-5 membrane with Si/Sn ratio of 25 showed a separation factor of 7.7 with a total flux of 0.49 $kg \cdot m^{-2} \cdot h^{-1}$ for a 5 wt% acetic acid aqueous solution at 363 K. Sebastian et al. [19] prepared Ti-ZSM-5 membrane with different Ti/Si ratio by MW-assisted hydrothermal heating method, and the membrane with Ti/Si ratio of 50 showed the highest separation factor of 65 with a flux of 2.2 $kg \cdot m^{-2} \cdot h^{-1}$ for 5 wt% ethanol/water mixtures at 338 K. Chen et al. [21] prepared zirconium silicalite-1 zeolite membrane to separating 5 wt% ethanol/water mixtures at 333 K, and the membrane showed high ethanol permselectivity with a flux of 1.01 $kg \cdot m^{-2} \cdot h^{-1}$ accompanied with a separation factor of 73.

MFI type zeolite belongs to pentasil family and contains straight channels (5.3 Å×5.6 Å) intersected by sinusoidal channels (5.5 Å×

†To whom correspondence should be addressed.
E-mail: zjwyz@cczu.edu.cn

5.1 Å). As another member of the pentasil family, MEL type zeolite only contains intersecting straight channels with pore sizes of 5.4 Å×5.3 Å. Both high-silica MFI and MEL zeolite membranes could be used in organics recovery due to the unique channel structure and hydrophobicity. Studies have shown that in MFI zeolite the diffusivity in the straight channels is relatively higher than in the sinusoidal channels [22,23]. According to this, Kosinov et al. [24] prepared MEL zeolite membrane on $\alpha$-$Al_2O_3$ hollow fiber by a secondary growth method, and the flux of ethanol/water mixture reached 3.60 $kg \cdot m^{-2} \cdot h^{-1}$ which was higher than that of MFI zeolite membrane with similar quality and membrane thickness. This proved that the MEL zeolite membrane has more probability satisfying industrial applications of pervaporation separation.

Considering the advantages of MEL zeolite in channel structure compared with MFI, we can anticipate that heteroatom isomorphously substituted MEL zeolite membranes may have better separation performance. At present, titanium and zirconium both have demonstrated that they can improve the hydrophobicity of MFI membrane [19,21], but there have been no reports about titanium or zirconium-substituted MEL zeolite membranes. Considering our previous work [25-28], Ti-silicalite-2 and Zr-silicalite-2 membranes were synthesized by a secondary growth method to recover DMF from aqueous solution in this study. To the best of our knowledge, this is the first time to prepare these membranes, and the effects of isomorphous substitution, feed temperature, and feed concentration on pervaporation were investigated.

## EXPERIMENTAL

### 1. Preparation of Silicalite-2 Seeds

Seeds crystals were prepared through a hydrothermal growth as reported by Kosinov et al. [24]. The synthesis solution was obtained by mixing tetrabutylammonium hydroxide (TBAOH, 50 wt%, Aladdin) and distilled water. The tetraethylorthosilicate (TEOS, 97 wt%, Aladdin) was added into the above solution under stirring. The initial molar composition was 1TBAOH : 3TEOS : 36$H_2O$. After vigorous stirring overnight at room temperature, the clear solution was transferred into Teflon-lined stainless steel autoclave and heated for 72 h at 403 K. The obtained crystals were washed by three cycles of centrifugation and dried at 353 K for several hours. Finally, the crystals were calcined at 823 K for 8 h to remove templates in the zeolite pores with heating and cooling rates of 1 $K \cdot min^{-1}$.

### 2. Preparation of MEL Membrane

MEL zeolite membranes were prepared by a secondary growth method on the porous $\alpha$-$Al_2O_3$ discs (average pore size, ~0.2 μm; diameter, 31 mm; thickness, 2 mm; porosity, ~30%, Nanjing University of Technology). The silicalite-2 crystals were dispersed into fresh ethanol to form 0.5 wt% seed suspension. The $\alpha$-$Al_2O_3$ discs were seeded in the above-prepared seed suspension by dip-coating technique to form a continuous seed layer. Following that, the seeded supports were dried at 353 K for 2 h. Three seed coating times were needed in our work. All membranes were synthesized from above supports seeded with silicalite-2 crystals. The synthesis solutions for membrane formation were prepared by mixing tetrabutylammonium, tetraethylorthosilicate and distilled water according to preparation of synthesis solution for silicalite-2 seeds. The tetrabutyl titanate (TBOT, 80 wt%, Aladdin) and zirconium n-butoxide (ZBOT, 98 wt%, Aladdin) were added dropwise into the resulting solutions, respectively; before that, the TBOT and ZBOT were diluted with 2-propanol. The molar composition of synthesis solutions for membranes was 1TBAOH : 3TEOS : 100$H_2O$ : 0.09M, where M was TBOT and ZBOT, respectively. For comparison, the silicalite-2 membrane was also prepared with a synthesis solution of 1TBAOH : 3TEOS : 100$H_2O$. After vigorous stirring, the clear solutions were poured in Teflon-lined stainless steel autoclaves (100 ml), followed by placing the pre-seeded supports horizontally into the solution. The autoclaves were placed in a preheated oven at 423 K and kept there for 48 h. The resulting materials were washed by distilled water and dried at 353 K overnight. After three repeated synthesis cycles to increase the growth of crystals and reduce the defects, the as-synthesized membranes were impermeable to $N_2$ with the pressure drop of 0.1 MPa at room temperature. To remove templates, all the obtained membranes were calcined in air flow at 823 K for 8 h with heating and cooling rates of 1 $K \cdot min^{-1}$.

### 3. Characterization

X-ray diffraction (XRD, Rigaku D/MAX-2500PC) patterns of the zeolite crystals and MEL membranes were measured at room temperature from a diffractometer with Cu K$\alpha$ radiation ($\lambda$=0.15406 nm) operated at 40 kV and 100 mA. The framework vibration spectra of the MEL crystals collected from the bottom of the corresponding autoclave were characterized by Fourier transform infrared (FT-IR, Nicolet PROTEGE 460) spectroscopy using KBr pellets technology in the range of 400-4,000 $cm^{-1}$. The morphology of the MEL membranes was observed by scanning electron microscopy (SEM, JSM-6360LA) at an acceleration voltage of 30 kV. The adsorption isotherms of organics and water at 298 K in the MEL crystals were measured using an Intelligent Gravimetric Analyzer (IGA-100B) from Hiden Instruments after the samples were activated at 473 K under dynamic vacuum for 12 h.

The pervaporation property of the MEL membranes was evaluated by separating DMF/water binary mixtures. The effective membrane area was $5.3 \times 10^{-4}$ $m^2$. A mechanical vacuum pump evacuated the permeate side of the membrane to a pressure less than 500 Pa. The DMF/water binary mixtures were recirculated over the membrane at a rate of 20 ml/min. The permeate vapor was condensed and collected in liquid nitrogen cooled traps for a certain time. The concentration of both the feed and permeate was determined by gas chromatography (GC-950 Haixin, Shanghai, China). The permeation flux was determined by weighing the cold traps during the pervaporation test. The pervaporation performance of the membrane was evaluated in terms of the permeate flux and selectivity. The permeate flux J was calculated by Eq. (1):

$$J = \frac{M}{At} \tag{1}$$

where M is the weight of the permeate collected within time t, and A is the effective membrane area. The separation factor $\alpha$ was determined as follows:

$$\alpha = \frac{Y_{DMF}/Y_{water}}{X_{DMF}/X_{water}} \tag{2}$$

where X and Y denote the mass fractions of components DMF

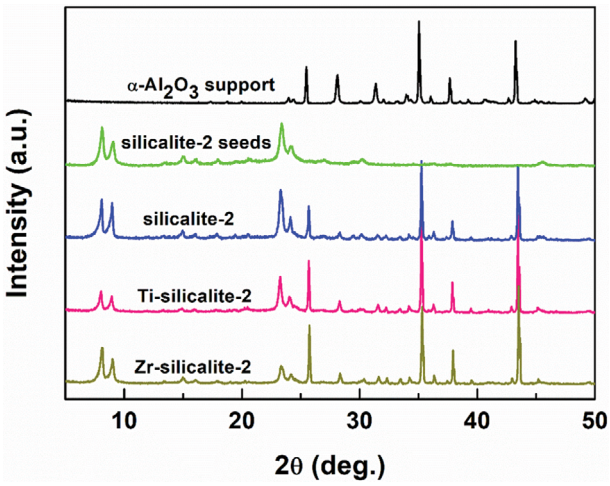


**Fig. 1. XRD patterns of $\alpha$-$Al_2O_3$ support, silicalite-2 seeds and MEL membranes.**

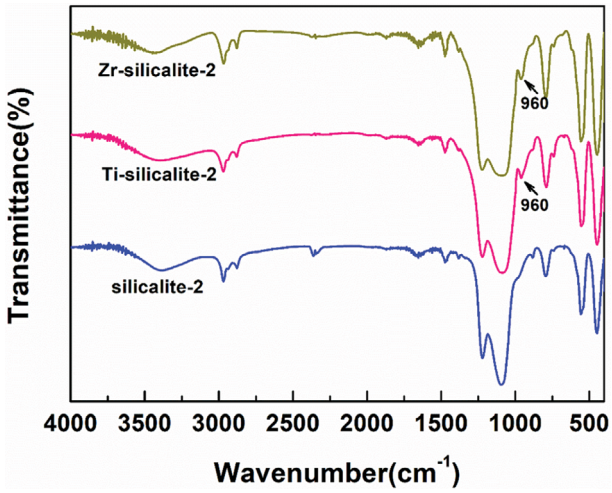


**Fig. 2. FT-IR spectra of MEL crystals.**

**Table 1. Crystal lattice parameters and unit cell volumes of MEL membranes calculated from XRD patterns**

| MEL crystals | a [Å] | b [Å] | c [Å] | V [Å$^3$] |
|---|---|---|---|---|
| Silicalite-2 | 20.2216 | 20.2216 | 13.5134 | 5,525.8135 |
| Ti-silicalite-2 | 20.2367 | 20.2367 | 13.5250 | 5,538.7500 |
| Zr-silicalite-2 | 20.2628 | 20.2628 | 13.5413 | 5,559.8014 |

and water in the feed and permeate sides, respectively.

## RESULTS AND DISCUSSION

### 1. Characterization of Silicalite-2 Seeds and MEL Membranes

Fig. 1 shows the XRD patterns of $\alpha$-$Al_2O_3$ support, silicalite-2 seeds and MEL membranes. The XRD reflections of the synthesized seeds exhibited characteristic peaks of MEL structure in the range of $2\theta$=7-9° and $2\theta$=23-25°, demonstrating the formation of silicalite-2 crystals [29]. The diffraction peaks of MEL structure and $\alpha$-$Al_2O_3$ were both observed in the XRD patterns of MEL membranes, and no obvious impurity phase was found, which proved that the MEL membranes were successfully prepared on the $\alpha$-$Al_2O_3$ support. The crystal lattice parameters and unit cell volumes of MEL membranes are given in Table 1. The lattice parameters and cell volumes were calculated according to the Bragg equation, $d=\lambda/\sin\theta$, where d denotes the spacing between the planes in the atomic lattice (a, b, c), $\lambda$ is the wavelength of used Cu K$\alpha$ radiations of 0.15406 nm and $\theta$ is observed XRD diffraction angle. As shown in Table 1, the lattice parameters and cell volumes of Ti-silicalite-2 and Zr-silicalite-2 membranes were larger than those of silicalite-2 membrane, which suggests that larger atoms (Ti, Zr) were incorporated into MEL framework. Besides, the parameters (a, b, c and V) of Ti-silicalite-2 were smaller than those of Zr-silicalite-2, which was consistent with the ion radius of $Ti^{4+}$ (0.061 nm) and $Zr^{4+}$ (0.072 nm). This further proved that Ti and Zr atoms were introduced into the zeolite structure and caused the increase of crystal lattice parameters and unit cell volumes.

IR spectra of MEL crystals are shown in Fig. 2. It can be seen

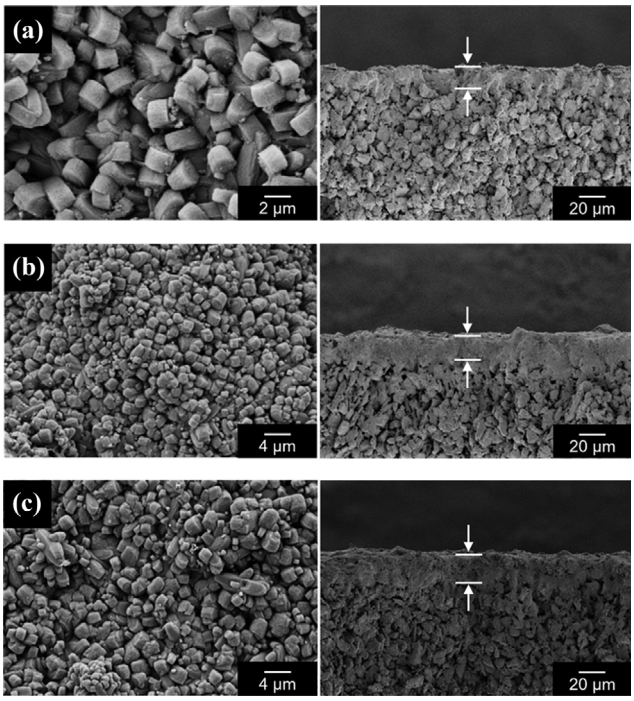


**Fig. 3. SEM images of the MEL membranes surface and cross-section ((a) silicalite-2; (b) Ti-silicalite-2; (c) Zr-silicalite-2).**

that all spectra have adsorption bands at around 1,220, 1,090, 795, 557 and 450 $cm^{-1}$, which was typical from MEL zeolites [30]. The bands at 1,220 and 1,090 $cm^{-1}$ were assigned to external asymmetric stretch and internal asymmetric stretch of the framework $TO_4$, respectively. The band at 795 $cm^{-1}$ was related to the external symmetric stretching of Si-O-T linkage. The framework vibration at 557 $cm^{-1}$ (double 5-ring) was characteristic of MEL-type zeolites. The absorption band observed at around 450 $cm^{-1}$ was assigned to T-O bend. Ti-silicalite-2 and Zr-silicalite-2 crystals both exhibited a weak band near 960 $cm^{-1}$. It can be assigned to Ti-O-Si or Zr-O-Si symmetric stretching vibration [21,31]. These indicate the presence of framework Ti and Zr in the Ti-silicalite-2 and Zr-sili-

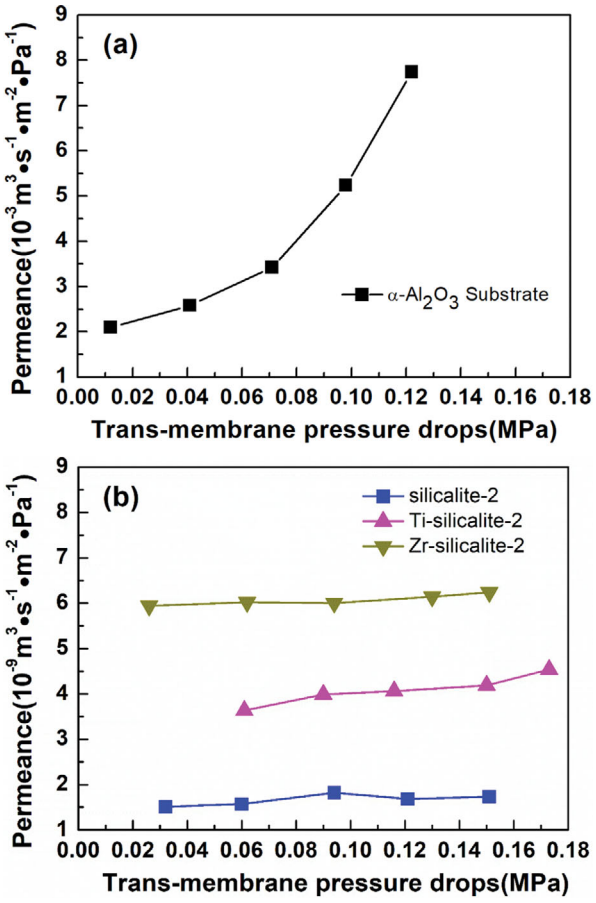


**Fig. 4. Permeance of $N_2$ through the $\alpha$-$Al_2O_3$ support and MEL membranes ((a) $\alpha$-$Al_2O_3$ support; (b) MEL membranes).**

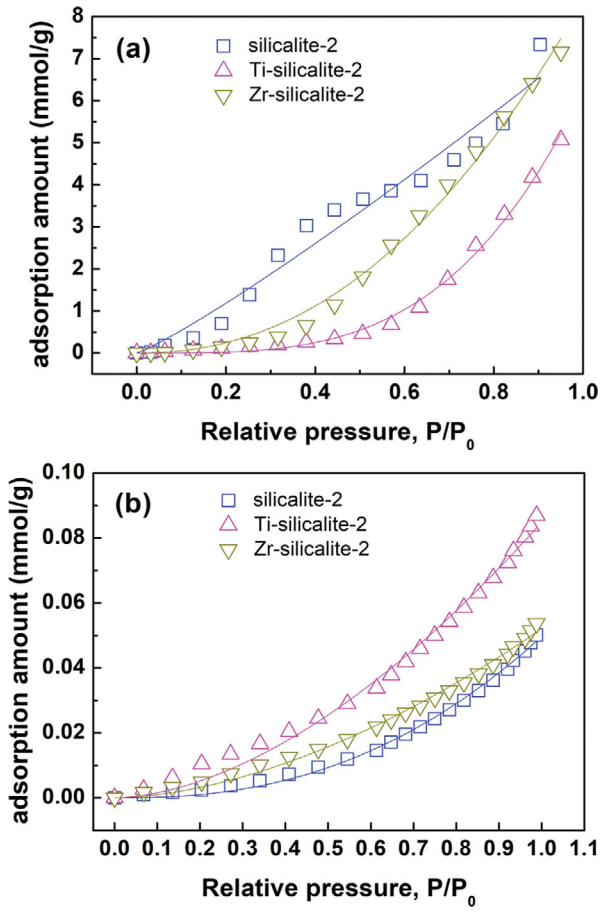


**Fig. 5. Adsorption isotherms of water and DMF on MEL crystals at 298 K ((a) Water; (b) DMF). Thin lines represent the fits to the Freundlich adsorption model.**

calite-2 zeolite, respectively.

Fig. 3 shows the surface and cross-section SEM images of silicalite-2, Ti-silicalite-2 and Zr-silicalite-2 membranes, respectively. The SEM images of porous $\alpha$-$Al_2O_3$ support were present in our previous work [32]. The top-view SEM images of membranes indicate that continuous and compact crystals were formed on top surface of $\alpha$-$Al_2O_3$ supports. It can be seen that three types of crystals were not exactly the same and the average grain sizes were in the range of 1-2 μm. Compared with the silicalite-2 and Zr-silicalite-2, the crystals of Ti-silicalite-2 membrane were slightly more uniform and compact. Meanwhile, the cross-section SEM images show that the membrane layers were compact and tightly adhered to the top of the $\alpha$-$Al_2O_3$ supports and the thickness of each membrane was approximately 20 μm.

In the process of pervaporation separation, the integrity of zeolite membrane substantially determines the effect of separation performance. Fig. 4 shows the single gas permeance of $N_2$ through the $\alpha$-$Al_2O_3$ support and MEL membranes as a function of trans-membrane pressure difference. As the trans-membrane pressure difference increased, the $N_2$ permeance of the $\alpha$-$Al_2O_3$ support showed an increasing trend, which demonstrated the existence of viscous/Poiseuille flow. After several times synthesis cycle, the $N_2$ permeance of MEL membranes was far less than that of $\alpha$-$Al_2O_3$ support, as shown in Fig. 4(b). The $N_2$ permeance of MEL membranes was almost independent of trans-membrane pressure difference, which implied that the prepared MEL membranes were integral and crack-free.

To test the hydrophilicity and hydrophobicity of MEL crystals, the adsorption amount of water and DMF in crystals under different relative pressure was measured as shown in Fig. 5. Fig. 5(a) presents the adsorption isotherms of water on three crystals at 298 K. As the relative pressure ($P/P_0$) approaches 1, the adsorption capacity of water on silicalite-2, Ti-silicalite-2 and Zr-silicalite-2 crystals could reach 7.334 mmol/g, 5.069 mmol/g and 7.159 mmol/g, respectively. Meanwhile, the adsorption amount of water on silicalite-2 crystal was higher than that on the other two MEL crystals in most relative pressure ranges. This indicated that the silicalite-2 zeolite was more hydrophilic than MEL crystals substituted by titanium and zirconium. Fig. 5(b) shows the adsorption isotherms of DMF in MEL crystals. It can be seen that the adsorption curve of DMF shows a steady increase on each MEL crystal. When pressure was close to the saturation vapor pressure of DMF, the adsorption capacity of DMF on silicalite-2, Ti-silicalite-2 and Zr-silicalite-2 crystals could reach 0.050 mmol/g, 0.087 mmol/g and 0.054 mmol/g, respectively. The adsorption amount of DMF on the Ti-silicalite-2 crystal was significantly higher than the amounts on the other two MEL crystals, which indicates that Ti-silicalite-2 crystal has stronger adsorption performance to DMF molecule.

**Table 2. Fitting parameters of Freundlich model onto MEL crystals at 298 K**

| MEL crystals | Water | | | DMF | | |
|---|---|---|---|---|---|---|
| | $K_f$ | n | $R^2$ | $K_f$ | n | $R^2$ |
| Silicalite-2 | 7.3651 | 0.8815 | 0.9672 | 0.0497 | 0.4154 | 0.9960 |
| Ti-silicalite-2 | 6.2526 | 0.2840 | 0.9952 | 0.0848 | 0.5772 | 0.9918 |
| Zr-silicalite-2 | 8.3630 | 0.4561 | 0.9938 | 0.0520 | 0.5795 | 0.9939 |

The Freundlich model is an empirical equation widely used in the research of multilayer adsorption on heterogeneous surfaces [33]. This model assumes that as the adsorbate pressure increases so too does the concentration of adsorbate on the adsorbent surface. Therefore, there is no maximum adsorption capacity. To reveal the adsorption behavior, the Freundlich model was utilized to fit the adsorption isotherms of water and DMF. The Freundlich equation is as follows:

$$q_e=K_f p^{1/n} \quad (3)$$

where $q_e$ is the equilibrium adsorption capacity, p is the adsorbate pressure, $K_f$ and n are the Freundlich constants representing the adsorption capacity and the adsorption intensity, respectively. The fitting lines of Freundlich model are shown in Fig. 5 and the detailed fitting parameters are summarized in Table 2. The fitting results indicate that the adsorption data are well-adjusted to the Freundlich model. Although the adsorption amount of water was higher than that of DMF in the single component adsorption experiment, the values of constant n reveal that the adsorption intensity of Ti-silicalite-2 and Zr-silicalite-2 crystals for DMF is greater than that for water and the competitive adsorption between water and DMF molecule plays a key role in the process of pervaporation separation.

## 2. Pervaporation Performance of the MEL Membranes

### 2-1. The Effect of Heteroatom Isomorphous Substitution

Table 3 shows the pervaporation performance of different MEL membranes for 5 wt% DMF/water binary mixtures at 343 K. The experimental results of pervaporation show that the DMF component preferentially permeated through these MEL membranes. Adsorption intensity and diffusion rate are primarily responsible for the final selectivity [34,35]. According to the solution-diffusion model, in the process of pervaporation, DMF molecules were preferentially adsorbed on the surface of MEL membranes and inhibited the permeation of water molecules [36-38]. The isomorphous substitution of Ti and Zr atoms improved the solubility and diffusivity of DMF in MEL membranes to varying degrees, as shown in Table S1. The Ti-silicalite-2 membrane has the highest DMF selectivity, which was due to its highest solubility of DMF and consistent with its highest adsorption capacity of DMF in Fig. 5(b). Meanwhile, heteroatom isomorphous substitution can adjust the zeolite pore size by changing the bond length and angle of T-O-Si (T=Ti and Zr) [39]. Because the ion radius follows $Zr^{4+}$ (0.072 nm)>$Ti^{4+}$ (0.061 nm)>$Si^{4+}$ (0.040 nm), the Zr-silicalite-2 membrane has the biggest zeolite pore size, further contributing to the highest diffusivity. However, the permeation fluxes and separation factor of silicalite-2 membrane were the lowest due to the low adsorption and diffusivity of DMF.

**Table 3. Pervaporation performance of the MEL membranes for 5 wt% DMF/water binary mixtures at 343 K**

| Membrane | Flux [$kg \cdot m^{-2} \cdot h^{-1}$] | Separation factor [-] |
|---|---|---|
| Silicalite-2 | 0.87±0.05 | 2.4±0.3 |
| Ti-silicalite-2 | 0.98±0.06 | 6.4±0.4 |
| Zr-silicalite-2 | 1.12±0.04 | 4.3±0.3 |

### 2-2. The Effect of Feed Temperature

Feed temperature has a significant effect on membrane flux and separation factor. Due to the best separation performance for DMF/water mixtures, the Ti-silicalite-2 membrane was used to investigate the effect of feed temperature on the separation performance in pervaporation. Fig. 6 shows the effect of feed temperature on separation performance for separating 5 wt% DMF/water mixtures. The total flux of DMF/water mixture increased from 0.43 to 0.98 $kg \cdot m^{-2} \cdot h^{-1}$ with feed temperature increasing from 303 to 343 K. The separation factor also increased from 2.3 to 6.4 under this temperature range. Increasing temperature can accelerate the molecule diffusion rate and reduce the adsorption amount [37,40]. Both DMF and water flux slowly increased, but the ratio of DMF to water also increased with temperature increasing. The change trends in partial fluxes led to the increase of total flux and separation factor. In addition, the DMF flux was lower than the water flux in this temperature range. This is because the larger kinetic diameter of DMF reduces the molecule diffusion rate in zeolite channel, but the competitive adsorption still dominates the preferential selectivity of membranes and the adsorbed DMF molecules inhibited the permeation of water molecules.

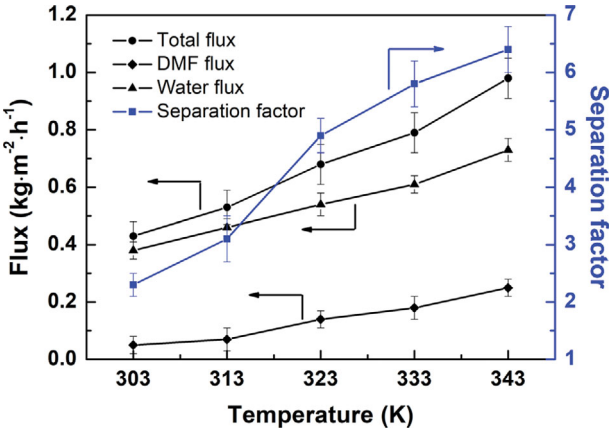


**Fig. 6. The effect of feed temperature on the separation performance for recovery of DMF from 5 wt% DMF/water mixtures through Ti-silicalite-2 membrane.**

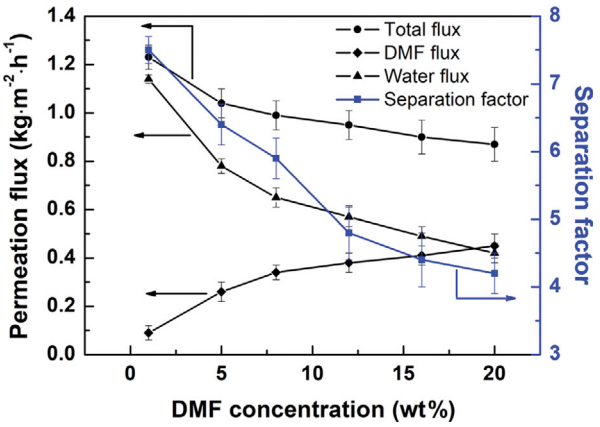


**Fig. 7. The effect of feed concentration on the separation performance for recovery of DMF from DMF/water mixtures through Ti-silicalite-2 membrane at 343 K.**

2-3. The Effect of Feed Concentration

Fig. 7 shows the effect of feed concentration on the separation performance for recovery of DMF from DMF/water mixtures through the Ti-silicalite-2 membrane at 343 K. As DMF concentration increased from 1 to 20 wt%, the total flux decreased gradually from 1.23 to 0.87 $kg \cdot m^{-2} \cdot h^{-1}$, and the separation factor decreased from 7.5 to 4.2. Meanwhile, the DMF flux increased from 0.09 to 0.45 $kg \cdot m^{-2} \cdot h^{-1}$, and the water flux decreased from 1.14 to 0.42 $kg \cdot m^{-2} \cdot h^{-1}$. As the feed concentration approached 20 wt%, the increase of DMF flux became slow. This suggests that the DMF adsorption amount on Ti-silicalite-2 membrane approached saturation and dynamic equilibrium with the diffusion rate. Besides, the increasing DMF adsorption coverage blocked the water molecule permeation and led to the decrease of water flux. As shown in Fig. 7, the decrease of water flux was faster than the increase of DMF flux; thus the total flux decreased with the increasing feed concentration. The separation factor decreased as feed concentration increased, because the DMF coverage on the feed side did not increase in proportional to the feed concentration [40].

**3. Comparison with Literature Data**

Table 4 summarizes the separation performance of MFI and MEL membranes in our previous and this work. In our previous work, the heteroatom isomorphously substituted MFI type zeolite membranes were synthesized for recovering DMF from its aqueous solution [27]. But the separation performance of MFI membranes was slightly worse than that of MEL membranes. The silicalite-2 and Sn-silicalite-2 membranes were also synthesized and showed a certain DMF selectivity [26,28]. In this work, the isomorphous substitution of Zr and Ti further enhanced the flux and separation factor of MEL zeolite membranes, and this presented a potential option for the application in recovery of DMF solvents.

## CONCLUSIONS

The heteroatom isomorphously substituted MEL zeolite membranes were synthesized on alumina ceramics discs by a secondary growth method. The effects of heteroatom isomorphous substitution, feed temperature and concentration on the separation performances were systematically investigated. The incorporation of heteroatom into MEL framework significantly enhanced the hydrophobicity of zeolite membranes and improved separation performance for DMF/water binary mixtures by pervaporation. The fluxes and separation factors for DMF/water binary mixtures both increased with the increasing feed temperature, and decreased with the increasing feed concentration. The Ti-silicalite-2 membrane exhibited high a separation factor of 6.4 with a total flux of 0.98 $kg \cdot m^{-2} \cdot h^{-1}$ for 5 wt% DMF/water mixture at 343 K.

## ACKNOWLEDGEMENT

This work was supported by Natural Science Foundation of Jiangsu Province (BK20200982), Natural Science Foundation of the Jiangsu Higher Education Institutions of China (18KJA530001), Advanced Catalysis and Green Manufacturing Collaborative Innovation Center, Changzhou University, A Project Funded by the Priority Academic Program Development of Jiangsu Higher Education Institutions (PAPD), and State Key Laboratory of Materials-Oriented Chemical Engineering.

## DISCLOSURE STATEMENT

The authors declare that they have no conflict of interest.

## SYMBOLS USED

A : effective membrane area [$m^2$]
d : spacing between the planes in the atomic lattice [Å]
J : permeate flux [$kg \cdot m^{-2} \cdot h^{-1}$]

**Table 4. Pervaporation performance of MEL membranes for DMF/water binary mixtures reported in the literature and in this work**

| Membrane | Feed concentration [wt%] | Feed temperature [K] | Membrane thickness [μm] | Flux [$kg \cdot m^{-2} \cdot h^{-1}$] | Separation factor [-] | Reference |
|---|---|---|---|---|---|---|
| Co-silicalite-1 | 5 | 313 | 40-50 | 0.66 | 4.4 | [27] |
| Fe-silicalite-1 | 5 | 313 | 40-50 | 0.84 | 2.9 | [27] |
| silicalite-2 | 5 | 343 | 20 | 0.87 | 2.4 | [26] |
| Sn-silicalite-2 | 5 | 343 | 40 | 0.99 | 5.6 | [28] |
| Zr-silicalite-2 | 5 | 343 | 20 | 1.12±0.04 | 4.3±0.3 | This work |
| Ti-silicalite-2 | 5 | 343 | 20 | 0.98±0.06 | 6.4±0.4 | This work |

$K_f$ : Freundlich constant [-]
M : weight of the permeate [kg]
n : Freundlich constant [-]
p : adsorbate pressure [mbar]
$q_e$ : equilibrium adsorption capacity [mmol·g$^{-1}$]
$R^2$ : correlation coefficient [-]
t : time [h]
v : unit cell volume [Å$^3$]
X : mass fraction of feed [-]
Y : mass fraction of permeate [-]

**Greek Letter**

α : separation factor [-]
θ : X-ray diffraction angle [°]
λ : wavelength [nm]

**Abbreviations**

BEA : Beta-Type
CHA : chabazite
DMF : dimethylformamide
FAU : faujasite
FT-IR : Fourier transform infrared
GC : gas chromatography
IGA : intelligent gravimetric analyzer
LTA : Linde-Type A
MEL : Mobil eleven
MFI : Mobil five
MOR : mordenite
MW : microwave
NaA : Natrium A
SEM : scanning electron microscopy
TBAOH : tetrabutylammonium hydroxide
TBOT : tetrabutyl titanate
TEOS : tetraethylorthosilicate
XRD : X-ray diffraction
ZBOT : zirconium n-butoxide

## SUPPORTING INFORMATION

Additional information as noted in the text. This information is available via the Internet at http://www.springer.com/chemistry/journal/11814.

## REFERENCES


1. S. Das, A. K. Banthia and B. Adhikari, *Desalination*, **197**, 106 (2006).
2. S.-L. Wee, C.-T. Tye and S. Bhatia, *Sep. Purif. Technol.*, **63**, 500 (2008).
3. X. Feng and R. Y. M. Huang, *Ind. Eng. Chem. Res.*, **36**, 1048 (1997).
4. Q. Liu, R. D. Noble, J. L. Falconer and H. H. Funke, *J. Membr. Sci.*, **117**, 163 (1996).
5. P. Shao and R. Y. M. Huang, *J. Membr. Sci.*, **287**, 162 (2007).
6. A. Çalhan, S. Deniz, J. Romero and A. Hasanoğlu, *Korean J. Chem. Eng.*, **36**, 1489 (2019).
7. J. Wang, W. Zhang, W. Li and W. Xing, *Korean J. Chem. Eng.*, **32**, 1369 (2015).
8. Z. Wang, Q. Ge, J. Shao and Y. Yan, *J. Am. Chem. Soc.*, **131**, 6910 (2009).
9. J. Jiang, L. Wang, L. Peng, C. Cai, C. Zhang, X. Wang and X. Gu, *J. Membr. Sci.*, **527**, 51 (2017).
10. H. Kita, *Membrane*, **20**, 169 (1995).
11. M. Torres, M. Gutiérrez, V. Mugica, M. Romero and L. López, *Catal. Today*, **166**, 205 (2011).
12. S. Aguado, J. Gascon, D. Farrusseng, J. C. Jansen and F. Kapteijn, *Micropor. Mesopor. Mater.*, **146**, 69 (2011).
13. F. Zhang, L. Xu, N. Hu, N. Bu, R. Zhou and X. Chen, *Sep. Purif. Technol.*, **129**, 9 (2014).
14. Z. Chen, D. Yin, Y. Li, J. Yang, J. Lu, Y. Zhang and J. Wang, *J. Membr. Sci.*, **369**, 506 (2011).
15. D. Korelskiy, T. Leppäjärvi, H. Zhou and M. Grahn, *J. Membr. Sci.*, **427**, 381 (2013).
16. T. Bowen, *J. Membr. Sci.*, **215**, 235 (2003).
17. L. Chai, H. Li, X. Zheng, J. Wang, J. Yang, J. Lu, D. Yin and Y. Zhang, *J. Membr. Sci.*, **491**, 168 (2015).
18. W. Sun, X. Wang, J. Yang, J. Lu, H. Han, Y. Zhang and J. Wang, *J. Membr. Sci.*, **335**, 83 (2009).
19. V. Sebastian, J. Motuzas, R. W. J. Dirrix, R. A. Terpstra, R. Mallada and A. Julbe, *Sep. Purif. Technol.*, **75**, 249 (2010).
20. S. Li, V. A. Tuan, J. L. Falconer and R. D. Noble, *Micropor. Mesopor. Mater.*, **58**, 137 (2003).
21. P. Chen, X. Chen, X. Chen, Z. An and H. Kita, *Chin. J. Chem.*, **27**, 1692 (2009).
22. S. Li, V. A. Tuan, R. D. Noble and J. L. Falconer, *AIChE J.*, **48**, 269 (2002).
23. L. Song and L. V. C. Rees, *Micropor. Mesopor. Mater.*, **35**, 301 (2000).
24. N. Kosinov and E. J. M. Hensen, *J. Membr. Sci.*, **447**, 12 (2013).
25. Y. Cao, Q. Zhang, R. Xu and J. Zhong, *Ion Exchange & Adsorption*, **32**, 423 (2016).
26. Q. G. Wu, H. Shao, J. Zhong, Q. Zhang and R. Xu, *Modern Chem. Ind.*, **35**, 46 (2015).
27. H. Shao, Y. Zhou, J. Zhong, Q. G. Wu, Q. Zhang and B. Z. Yang, *J. Chem. Eng. Chinese U.*, **28**, 965 (2014).
28. Q. G. Wu, H. Shao, J. Zhong, Q. Zhang and R. Xu, *Modern Chem. Ind.*, **39**, 94 (2019).
29. G. T. Kokotailo, P. Chu, S. L. Lawton and W. M. Meier, *Nature*, **275**, 119 (1978).
30. Y. Cheng and S. Pan, *Mater. Lett.*, **100**, 289 (2013).
31. D. P. Serrano, M. A. Uguina, R. Sanz, E. Castillo, A. Rodríguez, P. Sánchez, *Micropor. Mesopor. Mater.*, **69**, 197 (2004).
32. Q. Wu, R. Xu, J. Li, Q. Zhang, J. Zhong, W. Huang and X. Gu, *J. Porous Mat.*, **22**, 1195 (2015).
33. H. M. F. Freundlich, *Z. Phys.Chem.*, **57**, 385 (1906).
34. J. G. Wijmans and R. W. Baker, *J. Membr. Sci.*, **107**, 1 (1995).
35. T. Bowen, *J. Membr. Sci.*, **225**, 165 (2003).
36. M. Nomura, T. Yamaguchi and S.-i. Nakao, *J. Membr. Sci.*, **144**, 161 (1998).
37. J. Z. Yang, Q. L. Liu and H. T. Wang, *J. Membr. Sci.*, **291**, 1 (2007).
38. V. A. Tuan, S. Li, J. L. Falconer and R. D. Noble, *J. Membr. Sci.*, **196**, 111 (2002).
39. H. Kosslick, V. A. Tuan, R. Fricke, C. Peuker, W. Pilz and W. Storek, *J. Phys. Chem.*, **97**, 796 (1993).
40. S. Li, V. A. Tuan, R. D. Noble and J. L. Falconer, *Ind. Eng. Chem. Res.*, **40**, 6165 (2001).